(Preprint) AAS 23-084

SPACECRAFT SIMULATION SOFTWARE IMPLEMENTATION OF GENERAL PRESCRIBED MOTION DYNAMICS OF TWO CONNECTED RIGID BODIES

L. Kiner[*], J. Vaz Carneiro[†], C. Allard[‡] and H. Schaub[§]

The dynamics of systems with multiple connected rigid bodies are inherently coupled and complicated to derive as the number of appended bodies and degrees of freedom of the system increases. Prior work in multi-body dynamics using the elegant back-substitution method is expanded to consider a spacecraft consisting of a rigid hub and a relative six-degree of freedom (6 DOF) connected secondary rigid body following prescribed motion. The problem can be reduced in number of degrees of freedom depending on the application without the need to re-derive the equations of motion. An angular momentum-based equation of motion development is considered for the dynamics formulation. The Basilisk astrodynamics simulation framework is used to implement and validate the dynamics using the conservation quantities of angular momentum and energy.

INTRODUCTION

The persistent growth of ambitious missions to space has prompted increasingly complex spacecraft concepts. Such spacecraft often consist of multiple rigid bodies that are connected to the central rigid spacecraft hub. Solar arrays, robotic manipulators, gimbal thrusters, and communication dishes are examples of such connected rigid spacecraft components. The dynamics of these multi-body systems are notably challenging to implement in software because of the resulting dynamic coupling between the rigid spacecraft elements. For example, the modeling of deployable solar arrays presents varying levels of complexity depending on the degree of dynamic intricacy considered. Hinged rigid body approaches have been be considered as well as higher-order dynamics modeling to incorporate flexible dynamics and global bending modes.[1,2] The Space Station Remote Manipulator System (SSRMS) consisting of eight links and seven active joints is another prominent example of the advances in multi-body dynamics development. In order to ignore structural deflections and rigid-body rates, the seven DOF robotic manipulator arm must move slowly white recruiting parallel processing for real-time implementation.[3] As a result of such intricate multi-body systems, the field of multi-body dynamics has been widely studied for several decades.[1,4–6]

[*]Graduate Research Assistant, Ann and H.J. Smead Department of Aerospace Engineering Sciences, University of Colorado Boulder, Colorado Center For Astrodynamics Research, Boulder, CO, 80309. AAS Member, AIAA Member.

[†]Graduate Research Assistant, Ann and H.J. Smead Department of Aerospace Engineering Sciences, University of Colorado Boulder, Colorado Center For Astrodynamics Research, Boulder, CO, 80309. AAS Member.

[‡]Guidance, Navigation and Control Engineer, Laboratory for Atmospheric and Space Physics, 1234 Innovation Dr, Boulder, CO 80303, USA, Cody.Allard@lasp.colorado.edu

[§]Professor and Department Chair, Schaden Leadership Chair, Ann and H.J. Smead Department of Aerospace Engineering Sciences, University of Colorado, Boulder, 431 UCB, Colorado Center for Astrodynamics Research, Boulder, CO, 80309. AAS Fellow, AIAA Fellow.

For multi-body systems, the dynamics of each body both influence and are influenced by the motion of the other system bodies. Therefore, knowledge of the general spacecraft hub dynamics relies on integrating additional equations of motion for each of the appended bodies in the system. As more bodies are added to the system, the corresponding computational load for numerical integration increases. However, particular *prescribed* components exist whose dynamics are assumed to be independent of the motion of the other bodies in the system. Such components are considered to only influence the dynamics of the rest of the system, meaning they impact the motion of the spacecraft's rigid hub. This one-way dynamic coupling is characteristic of stepper motor-controlled articulable solar arrays, actuated platforms, gimbal thrusters, servo'd sensors, and high bandwidth control components. These spacecraft components are referred to as *prescribed bodies* in this paper. Moreover, it is not necessary to completely derive the equations of motion of such components if their motion is instead prescribed through a commanded reference trajectory. As a result, some degrees of freedom of the hub equations of motion may be eliminated for bodies with a priori known states.[3] This appropriately reduces the computational overhead for complex spacecraft simulations.

Previous work in multi-body prescribed motion dynamics has investigated a wide variety of applications. Ardakani and Bridges studied the dynamic coupling between a rigid vehicle following prescribed planar motion containing fluid and the fluid motion using Lagrangian Mechanics.[7] Gerrits and Veldman studied the same problem using Newtonian and Eulerian mechanics.[8,9] Jain and Rodriguez developed a recursive algorithm to model the dynamics of a serial-chain of hinges undergoing optional prescribed motion.[3] The formulated dynamics algorithm was applied to NASA's Cassini spacecraft, where it was used to model Cassini's articulated main engine and high precision scan platform in 2 DOF and probe relay antenna in 1 DOF.[3] The formulation is used in real-time aboard Cassini as part of its flexible multi-body dynamics simulation software package.[3]

This paper builds on previous multi-body prescribed dynamics work by developing a general method of prescribing the three-dimensional motion of a prescribed rigid body with respect to a spacecraft hub. This work further advances the current spacecraft simulation capability by implementing the derived general formulation modularly into the open-source Basilisk astrodynamics software package [*]. A spacecraft consisting of a rigid hub and a relative six-degree of freedom (6 DOF) connected prescribed rigid body is considered for the dynamics formulation. The prescribed body is mounted onto an interface that is fixed with respect to the hub. The prescribed body may be commanded to translate and rotate in three-dimensional space with respect to the interface it is mounted on. An angular momentum-based equation of motion development is considered and the derived translational and rotational dynamics are implemented Basilisk and validated using the conservation quantities of orbital angular momentum, orbital energy, and rotational angular momentum.

The organization of this paper is as follows. First, the required reference frame definitions for the dynamics derivation are established. Next, the 6 DOF translational and rotational equations of motion for a spacecraft consisting of a rigid hub and connected prescribed body following prescribed motion are presented. The software implementation of the derived multi-body dynamics and the translational and rotational motion flight software profilers are next outlined. The simulation results are then presented along with the dynamics validation. The concluding remarks are given in the final section.

[*] `https://hanspeterschaub.info/basilisk/index.html`

PROBLEM STATEMENT

The spacecraft geometry of interest for this derivation is illustrated in Fig. (1):

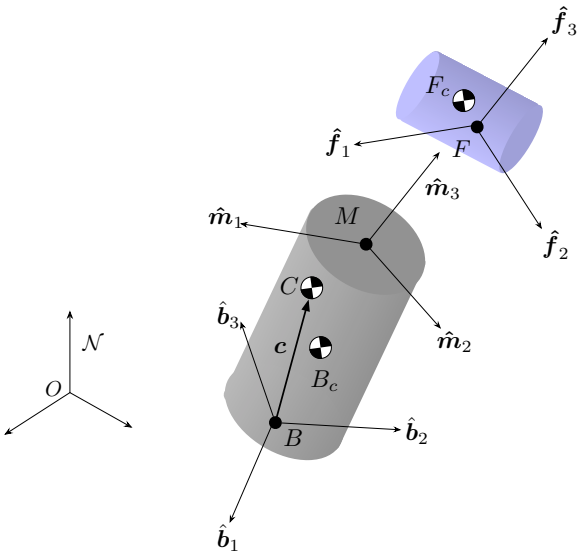

Figure 1. Spacecraft geometry, variables, and coordinate frames used for this derivation.

The four coordinate frames required for the following derivation are as follows. The spacecraft hub dynamics are developed with respect to an inertial reference frame indicated by $\mathcal{N}$: $\{N, \hat{\boldsymbol{n}}_1, \hat{\boldsymbol{n}}_2, \hat{\boldsymbol{n}}_3\}$. The spacecraft body frame $\mathcal{B} : \{B, \hat{\boldsymbol{b}}_1, \hat{\boldsymbol{b}}_2, \hat{\boldsymbol{b}}_3\}$ describes the motion of the spacecraft hub. The origin of this frame is located at a body-fixed point B. The point B_c is defined as the center of mass of the hub. The prescribed body frame $\mathcal{F} : \{F, \hat{\boldsymbol{f}}_1, \hat{\boldsymbol{f}}_2, \hat{\boldsymbol{f}}_3\}$ is the frame that describes the motion of the prescribed body attached to the spacecraft hub through the mount interface. The origin of this frame is located at the point F that is body-fixed to the prescribed body. The point F_c is defined as the center of mass of the prescribed body. The mount frame $\mathcal{M} : \{M, \hat{\boldsymbol{m}}_1, \hat{\boldsymbol{m}}_2, \hat{\boldsymbol{m}}_3\}$ is located on and fixed with respect to the spacecraft hub. The origin of the mount frame is located at a body-fixed point M. The mount frame serves as an intermediate frame that aids in describing the motion of the prescribed body with respect to the spacecraft body frame.

DERIVATION OF EQUATIONS OF MOTION

This section derives the spacecraft translational and rotational equations of motion using Newtonian and Eularian mechanics. This approach is desired because the derived equations are general, compact, and directly express the spacecraft hub dynamics. Accordingly, the equations of motion are straightforward to implement and validate in software.

Spacecraft Translational Equations of Motion

The spacecraft hub translational equations of motion are derived beginning with Newton's second law for the spacecraft center of mass:[10]

$$m_{\text{sc}} \ddot{\boldsymbol{r}}_{C/N} = \sum \boldsymbol{F}_{ext} \tag{1}$$

where

$$\ddot{\boldsymbol{r}}_{C/N} = \ddot{\boldsymbol{r}}_{B/N} + \ddot{\boldsymbol{c}} \tag{2}$$

To solve for $\ddot{\boldsymbol{c}}$, first the vector $\boldsymbol{c}$ must be defined:

$$\boldsymbol{c} = \frac{m_{\text{hub}}\boldsymbol{r}_{B_c/B} + m_{\text{P}}\boldsymbol{r}_{F_c/B}}{m_{\text{sc}}} \tag{3}$$

Next the body-frame time derivative of $\boldsymbol{c}$ is taken.

$$\boldsymbol{c}' = \frac{m_{\text{hub}}\boldsymbol{r}'_{B_c/B} + m_{\text{P}}\boldsymbol{r}'_{F_c/B}}{m_{\text{sc}}} \tag{4}$$

Eq. (4) may be further simplified with the assumption that the hub center of mass is body-fixed ($\boldsymbol{r}'_{B_c/B} = 0$):

$$\boldsymbol{c}' = \frac{m_{\text{P}}\boldsymbol{r}'_{F_c/B}}{m_{\text{sc}}} \tag{5}$$

where $\boldsymbol{r}'_{F_c/B}$ may be defined as:

$$\boldsymbol{r}'_{F_c/B} = \boldsymbol{r}'_{F_c/F} + \boldsymbol{r}'_{F/M} + \boldsymbol{r}'_{M/B} = \boldsymbol{r}'_{F_c/F} + \boldsymbol{r}'_{F/M} \tag{6}$$

Note above that point M is body-fixed ($\boldsymbol{r}'_{M/B} = 0$). Expanding the body-frame derivative of $\boldsymbol{r}_{F_c/F}$ gives:

$$\boldsymbol{r}'_{F_c/F} = \frac{{}^{\mathcal{F}}\text{d}}{\text{d}t}\left(\boldsymbol{r}_{F_c/F}\right) + \boldsymbol{\omega}_{\mathcal{F}/\mathcal{B}} \times \boldsymbol{r}_{F_c/F} = \boldsymbol{\omega}_{\mathcal{F}/\mathcal{B}} \times \boldsymbol{r}_{F_c/F} \tag{7}$$

Note that the vector $\boldsymbol{r}_{F_c/F}$ is constant in the F-frame. Further simplification of Eq. (6) using Eq. (7) gives:

$$\boldsymbol{r}'_{F_c/B} = [\tilde{\boldsymbol{\omega}}_{\mathcal{F}/\mathcal{B}}]\boldsymbol{r}_{F_c/F} + \boldsymbol{r}'_{F/M} \tag{8}$$

The second body-frame derivative of the center of mass position with respect to point B is:

$$\boldsymbol{c}'' = \frac{m_{\text{P}}\boldsymbol{r}''_{F_c/B}}{m_{\text{sc}}} \tag{9}$$

where $\boldsymbol{r}''_{F_c/B}$ may be defined as:

$$\boldsymbol{r}''_{F_c/B} = \boldsymbol{r}''_{F_c/F} + \boldsymbol{r}''_{F/M} = [\tilde{\boldsymbol{\omega}}'_{\mathcal{F}/\mathcal{B}}]\boldsymbol{r}_{F_c/F} + [\tilde{\boldsymbol{\omega}}_{\mathcal{F}/\mathcal{B}}]\boldsymbol{r}'_{F_c/F} + \boldsymbol{r}''_{F/M} = [\tilde{\boldsymbol{\omega}}'_{\mathcal{F}/\mathcal{B}}]\boldsymbol{r}_{F_c/F} + [\tilde{\boldsymbol{\omega}}_{\mathcal{F}/\mathcal{B}}]^2\boldsymbol{r}_{F_c/F} + \boldsymbol{r}''_{F/M} \tag{10}$$

Further simplification of Eq. (10) yields the final result:

$$\boldsymbol{r}''_{F_c/B} = \left([\tilde{\boldsymbol{\omega}}'_{\mathcal{F}/\mathcal{B}}] + [\tilde{\boldsymbol{\omega}}_{\mathcal{F}/\mathcal{B}}]^2\right)\boldsymbol{r}_{F_c/F} + \boldsymbol{r}''_{F/M} \tag{11}$$

Next the inertial time derivative of $\boldsymbol{c}$ may be taken using the transport theorem:

$$\dot{\boldsymbol{c}} = \boldsymbol{c}' + \boldsymbol{\omega}_{\mathcal{B}/\mathcal{N}} \times \boldsymbol{c} \tag{12}$$

Taking the second time derivative of $\boldsymbol{c}$ gives:

$$\ddot{\boldsymbol{c}} = \dot{\boldsymbol{c}}^{'} + \boldsymbol{\omega}_{\mathcal{B}/\mathcal{N}} \times \dot{\boldsymbol{c}} \tag{13}$$

The term $\dot{\boldsymbol{c}}^{'}$ is expressed as:

$$\dot{\boldsymbol{c}}^{'} = \boldsymbol{c}^{''} + \left(\dot{\boldsymbol{\omega}}_{\mathcal{B}/\mathcal{N}} \times \boldsymbol{c}\right) + \left(\boldsymbol{\omega}_{\mathcal{B}/\mathcal{N}} \times \boldsymbol{c}^{'}\right) \tag{14}$$

Substituting Eqs. (12) and (14) into Eq. (13) yields:

$$\ddot{\boldsymbol{c}} = \boldsymbol{c}^{''} + \left(\dot{\boldsymbol{\omega}}_{\mathcal{B}/\mathcal{N}} \times \boldsymbol{c}\right) + \left(\boldsymbol{\omega}_{\mathcal{B}/\mathcal{N}} \times \boldsymbol{c}^{'}\right) + \boldsymbol{\omega}_{\mathcal{B}/\mathcal{N}} \times \left(\boldsymbol{c}^{'} + \boldsymbol{\omega}_{\mathcal{B}/\mathcal{N}} \times \boldsymbol{c}\right) \tag{15}$$

Further simplifying and expanding the above result yields:

$$\ddot{\boldsymbol{c}} = \boldsymbol{c}^{''} + 2\left(\boldsymbol{\omega}_{\mathcal{B}/\mathcal{N}} \times \boldsymbol{c}^{'}\right) + \left(\dot{\boldsymbol{\omega}}_{\mathcal{B}/\mathcal{N}} \times \boldsymbol{c}\right) + \boldsymbol{\omega}_{\mathcal{B}/\mathcal{N}} \times \left(\boldsymbol{\omega}_{\mathcal{B}/\mathcal{N}} \times \boldsymbol{c}\right) \tag{16}$$

Eq. (16) may be substituted into Eq. (2) to give the following result:

$$\ddot{\boldsymbol{r}}_{C/N} = \ddot{\boldsymbol{r}}_{B/N} + \boldsymbol{c}^{''} + 2\left(\boldsymbol{\omega}_{\mathcal{B}/\mathcal{N}} \times \boldsymbol{c}^{'}\right) + \left(\dot{\boldsymbol{\omega}}_{\mathcal{B}/\mathcal{N}} \times \boldsymbol{c}\right) + \boldsymbol{\omega}_{\mathcal{B}/\mathcal{N}} \times \left(\boldsymbol{\omega}_{\mathcal{B}/\mathcal{N}} \times \boldsymbol{c}\right) \tag{17}$$

Substitution of Eq. (17) into Eq. (1) gives the translational equations of motion of this system:

$$m_{\text{sc}}\left[\ddot{\boldsymbol{r}}_{B/N} + \boldsymbol{c}^{''} + 2\left(\boldsymbol{\omega}_{\mathcal{B}/\mathcal{N}} \times \boldsymbol{c}^{'}\right) + \left(\dot{\boldsymbol{\omega}}_{\mathcal{B}/\mathcal{N}} \times \boldsymbol{c}\right) + \boldsymbol{\omega}_{\mathcal{B}/\mathcal{N}} \times \left(\boldsymbol{\omega}_{\mathcal{B}/\mathcal{N}} \times \boldsymbol{c}\right)\right] = \boldsymbol{F}_{ext} \tag{18}$$

Bringing second-order derivatives to the left-hand side and substituting in Eq. (9) for $\boldsymbol{c}^{''}$ gives the desired form of the system translational equations of motion for software implementation:

$$m_{\text{sc}}\ddot{\boldsymbol{r}}_{B/N} + m_{\text{sc}}[\dot{\tilde{\boldsymbol{\omega}}}_{\mathcal{B}/\mathcal{N}}]\boldsymbol{c} = \boldsymbol{F}_{ext} - m_{\text{P}}\boldsymbol{r}^{''}_{F_c/B} - 2m_{sc}[\tilde{\boldsymbol{\omega}}_{\mathcal{B}/\mathcal{N}}]\boldsymbol{c}^{'} - m_{sc}[\tilde{\boldsymbol{\omega}}_{\mathcal{B}/\mathcal{N}}]^2\boldsymbol{c} \tag{19}$$

Spacecraft Rotational Equations of Motion

The derivation of the spacecraft hub rotational equations of motion begins with Euler's equation applied to the case where the angular momentum derivative is taken about a body-fixed point not coincident with the system center of mass:[10]

$$\dot{\boldsymbol{H}}_{\text{sc},B} = \boldsymbol{L}_B + m_{\text{sc}}(\ddot{\boldsymbol{r}}_{B/N} \times \boldsymbol{c}) \tag{20}$$

where $\boldsymbol{L}_B$ is the external torque acting on the spacecraft about point B. The angular momentum of the spacecraft about the body-fixed point B must first be defined:

$$\boldsymbol{H}_{\text{sc},B} = \boldsymbol{H}_{\text{hub},B} + \boldsymbol{H}_{\text{P},B} \tag{21}$$

The hub angular momentum about point B is:

$$\boldsymbol{H}_{\text{hub},B} = \boldsymbol{H}_{\text{hub},B_c} + m_{\text{hub}}(\boldsymbol{r}_{B_c/B} \times \dot{\boldsymbol{r}}_{B_c/B}) \tag{22}$$

where

$$\dot{\boldsymbol{r}}_{B_c/B} = \boldsymbol{r}^{'}_{B_c/B} + \boldsymbol{\omega}_{\mathcal{B}/\mathcal{N}} \times \boldsymbol{r}_{B_c/B} = \boldsymbol{\omega}_{\mathcal{B}/\mathcal{N}} \times \boldsymbol{r}_{B_c/B} \tag{23}$$

Note that the vector $\boldsymbol{r}_{B_c/B}$ is constant in the B-frame. The hub angular momentum about its center of mass point B_c is:

$$\boldsymbol{H}_{\text{hub},B_c} = [I_{\text{hub},B_c}]\boldsymbol{\omega}_{\mathcal{B}/\mathcal{N}} \tag{24}$$

Eq. (22) is rewritten using Eqs. (23) and (24):

$$\boldsymbol{H}_{\text{hub},B} = [I_{\text{hub},B_c}]\boldsymbol{\omega}_{\mathcal{B}/\mathcal{N}} + m_{\text{hub}}(\boldsymbol{r}_{B_c/B} \times \boldsymbol{\omega}_{\mathcal{B}/\mathcal{N}} \times \boldsymbol{r}_{B_c/B}) \tag{25}$$

Further simplification gives the intermediate result:

$$\boldsymbol{H}_{\text{hub},B} = [I_{\text{hub},B_c}]\boldsymbol{\omega}_{\mathcal{B}/\mathcal{N}} - m_{\text{hub}}[\tilde{\boldsymbol{r}}_{B_c/B}]^2\boldsymbol{\omega}_{\mathcal{B}/\mathcal{N}} = \left([I_{\text{hub},B_c}] - m_{\text{hub}}[\tilde{\boldsymbol{r}}_{B_c/B}]^2\right)\boldsymbol{\omega}_{\mathcal{B}/\mathcal{N}} \tag{26}$$

The above expression may finally be simplified to:

$$\boldsymbol{H}_{\text{hub},B} = [I_{\text{hub},B}]\boldsymbol{\omega}_{\mathcal{B}/\mathcal{N}} \tag{27}$$

Next, the prescribed body angular momentum about point B is:

$$\boldsymbol{H}_{\text{P},B} = \boldsymbol{H}_{\text{P},F_c} + m_{\text{P}}(\boldsymbol{r}_{F_c/B} \times \dot{\boldsymbol{r}}_{F_c/B}) \tag{28}$$

where

$$\dot{\boldsymbol{r}}_{F_c/B} = \boldsymbol{r}'_{F_c/B} + \boldsymbol{\omega}_{\mathcal{B}/\mathcal{N}} \times \boldsymbol{r}_{F_c/B} \tag{29}$$

The prescribed body angular momentum about its center of mass, point F_c is:

$$\boldsymbol{H}_{\text{P},F_c} = [I_{\text{P},F_c}]\boldsymbol{\omega}_{\mathcal{F}/\mathcal{N}} \tag{30}$$

Eq. (28) is rewritten using Eqs. (29) and (30):

$$\boldsymbol{H}_{\text{P},B} = [I_{\text{P},F_c}]\boldsymbol{\omega}_{\mathcal{F}/\mathcal{N}} + m_{\text{P}}\left(\boldsymbol{r}_{F_c/B} \times \left(\boldsymbol{r}'_{F_c/B} + \boldsymbol{\omega}_{\mathcal{B}/\mathcal{N}} \times \boldsymbol{r}_{F_c/B}\right)\right) \tag{31}$$

Simplifying Eq. (31) gives the intermediate result:

$$\boldsymbol{H}_{\text{P},B} = [I_{\text{P},F_c}]\boldsymbol{\omega}_{\mathcal{F}/\mathcal{N}} + m_{\text{P}}[\tilde{\boldsymbol{r}}_{F_c/B}]\boldsymbol{r}'_{F_c/B} - m_{\text{P}}[\tilde{\boldsymbol{r}}_{F_c/B}]^2\boldsymbol{\omega}_{\mathcal{B}/\mathcal{N}} \tag{32}$$

Further simplification yields:

$$\boldsymbol{H}_{\text{P},B} = [I_{\text{P},B}]\boldsymbol{\omega}_{\mathcal{B}/\mathcal{N}} + [I_{\text{P},F_c}]\boldsymbol{\omega}_{\mathcal{F}/\mathcal{B}} + m_{\text{P}}[\tilde{\boldsymbol{r}}_{F_c/B}]\boldsymbol{r}'_{F_c/B} \tag{33}$$

Eq. (21) can now be rewritten using Eqs. (27) and (33):

$$\boldsymbol{H}_{\text{sc},B} = [I_{\text{hub},B}]\boldsymbol{\omega}_{\mathcal{B}/\mathcal{N}} + [I_{\text{P},B}]\boldsymbol{\omega}_{\mathcal{B}/\mathcal{N}} + [I_{\text{P},F_c}]\boldsymbol{\omega}_{\mathcal{F}/\mathcal{B}} + m_{\text{P}}[\tilde{\boldsymbol{r}}_{F_c/B}]\boldsymbol{r}'_{F_c/B} \tag{34}$$

The hub and prescribed body inertias about point B are combined to give the spacecraft inertia about point B:

$$[I_{\text{sc},B}] = [I_{\text{hub},B}] + [I_{\text{P},B}] \tag{35}$$

Rewriting Eq. (34) using Eq. (35) gives:

$$\boldsymbol{H}_{\text{sc},B} = [I_{\text{sc},B}]\boldsymbol{\omega}_{\mathcal{B}/\mathcal{N}} + [I_{\text{P},F_c}]\boldsymbol{\omega}_{\mathcal{F}/\mathcal{B}} + m_{\text{P}}[\tilde{\boldsymbol{r}}_{F_c/B}]\boldsymbol{r}'_{F_c/B} \tag{36}$$

The inertial time derivative of the spacecraft angular momentum about point B can now be taken using the Transport Theorem:

$$\dot{\boldsymbol{H}}_{\text{sc},B} = \boldsymbol{H}'_{\text{sc},B} + \boldsymbol{\omega}_{\mathcal{B}/\mathcal{N}} \times \boldsymbol{H}_{\text{sc},B} \tag{37}$$

The body-frame derivative of the space vehicle angular momentum is expressed as:

$$\boldsymbol{H}'_{\text{sc},B} = [I'_{\text{sc},B}]\boldsymbol{\omega}_{\mathcal{B}/\mathcal{N}} + [I_{\text{sc},B}]\dot{\boldsymbol{\omega}}_{\mathcal{B}/\mathcal{N}} + [I'_{\text{P},F_c}]\boldsymbol{\omega}_{\mathcal{F}/\mathcal{B}} + [I_{\text{P},F_c}]\boldsymbol{\omega}'_{\mathcal{F}/\mathcal{B}} + m_{\text{P}}[\tilde{\boldsymbol{r}}_{F_c/B}]\boldsymbol{r}''_{F_c/B} \tag{38}$$

The body-frame derivative of the spacecraft inertia about point B can be expressed as:

$$[I'_{\text{sc},B}] = [I'_{\text{hub},B}] + [I'_{\text{P},B}] = [I'_{\text{P},B}] \tag{39}$$

Note that the hub inertia about point B is constant in the $\mathcal{B}$ frame. Next the body-frame derivative of the prescribed body inertia about point B may be defined. First recall that the inertia of the prescribed body about point B is defined as:

$$[I_{\text{P},B}] = [I_{\text{P},F_c}] + m_{\text{P}}[\tilde{\boldsymbol{r}}_{F_c/B}][\tilde{\boldsymbol{r}}_{F_c/B}]^T \tag{40}$$

Taking the body-frame derivative of Eq. (40):

$$[I'_{\text{P},B}] = [I'_{\text{P},F_c}] + m_{\text{P}}\left([\tilde{\boldsymbol{r}}'_{F_c/B}][\tilde{\boldsymbol{r}}_{F_c/B}]^T + [\tilde{\boldsymbol{r}}_{F_c/B}][\tilde{\boldsymbol{r}}'_{F_c/B}]^T\right) \tag{41}$$

The body-frame derivative of the first term in Eq. (41) may be evaluated using the Transport Theorem of the inertia tensor[11] noting that the prescribed body inertia about its center of mass F_c is constant in the F-frame:

$$[I'_{\text{P},F_c}] = \frac{^{\mathcal{F}}\text{d}}{\text{d}t}[I_{\text{P},F_c}] + [\tilde{\boldsymbol{\omega}}_{\mathcal{F}/\mathcal{B}}][I_{\text{P},F_c}] - [I_{\text{P},F_c}][\tilde{\boldsymbol{\omega}}_{\mathcal{F}/\mathcal{B}}] = [\tilde{\boldsymbol{\omega}}_{\mathcal{F}/\mathcal{B}}][I_{\text{P},F_c}] - [I_{\text{P},F_c}][\tilde{\boldsymbol{\omega}}_{\mathcal{F}/\mathcal{B}}] \tag{42}$$

Substituting Eq. (42) into Eq. (41) gives the final result:

$$[I'_{\text{P},B}] = [\tilde{\boldsymbol{\omega}}_{\mathcal{F}/\mathcal{B}}][I_{\text{P},F_c}] + [I_{\text{P},F_c}][\tilde{\boldsymbol{\omega}}_{\mathcal{F}/\mathcal{B}}] + m_{\text{P}}\left([\tilde{\boldsymbol{r}}'_{F_c/B}][\tilde{\boldsymbol{r}}_{F_c/B}]^T + [\tilde{\boldsymbol{r}}_{F_c/B}][\tilde{\boldsymbol{r}}'_{F_c/B}]^T\right) \tag{43}$$

Eq. (37) can now be rewritten as:

$$\dot{\boldsymbol{H}}_{\text{sc},B} = \boldsymbol{H}'_{\text{sc},B} + [\tilde{\boldsymbol{\omega}}_{\mathcal{B}/\mathcal{N}}][I_{\text{sc},B}]\boldsymbol{\omega}_{\mathcal{B}/\mathcal{N}} + [\tilde{\boldsymbol{\omega}}_{\mathcal{B}/\mathcal{N}}][I_{\text{P},F_c}]\boldsymbol{\omega}_{\mathcal{F}/\mathcal{B}} + m_{\text{P}}[\tilde{\boldsymbol{\omega}}_{\mathcal{B}/\mathcal{N}}][\tilde{\boldsymbol{r}}_{F_c/B}]\boldsymbol{r}'_{F_c/B} \tag{44}$$

Eq. (44) may be substituted into Eq. (20) to give the intermediate result for the system rotational equations of motion:

$$\begin{aligned}\boldsymbol{H}'_{\text{sc},B} + [\tilde{\boldsymbol{\omega}}_{\mathcal{B}/\mathcal{N}}][I_{\text{sc},B}]\boldsymbol{\omega}_{\mathcal{B}/\mathcal{N}} + [\tilde{\boldsymbol{\omega}}_{\mathcal{B}/\mathcal{N}}][I_{\text{P},F_c}]\boldsymbol{\omega}_{\mathcal{F}/\mathcal{B}} + m_{\text{P}}[\tilde{\boldsymbol{\omega}}_{\mathcal{B}/\mathcal{N}}][\tilde{\boldsymbol{r}}_{F_c/B}]\boldsymbol{r}'_{F_c/B} \\ = \boldsymbol{L}_B + m_{\text{sc}}(\ddot{\boldsymbol{r}}_{B/N} \times \boldsymbol{c})\end{aligned} \tag{45}$$

Substituting $\boldsymbol{H}'_{\text{sc},B}$ using Eq. (38) into the above equation gives:

$$\begin{aligned}[I'_{\text{sc},B}]\boldsymbol{\omega}_{\mathcal{B}/\mathcal{N}} + [I_{\text{sc},B}]\dot{\boldsymbol{\omega}}_{\mathcal{B}/\mathcal{N}} + [I'_{\text{P},F_c}]\boldsymbol{\omega}_{\mathcal{F}/\mathcal{B}} + [I_{\text{P},F_c}]\boldsymbol{\omega}'_{\mathcal{F}/\mathcal{B}} + m_{\text{P}}[\tilde{\boldsymbol{r}}_{F_c/B}]\boldsymbol{r}''_{F_c/B} \\ + [\tilde{\boldsymbol{\omega}}_{\mathcal{B}/\mathcal{N}}][I_{\text{sc},B}]\boldsymbol{\omega}_{\mathcal{B}/\mathcal{N}} + [\tilde{\boldsymbol{\omega}}_{\mathcal{B}/\mathcal{N}}][I_{\text{P},F_c}]\boldsymbol{\omega}_{\mathcal{F}/\mathcal{B}} + m_{\text{P}}[\tilde{\boldsymbol{\omega}}_{\mathcal{B}/\mathcal{N}}][\tilde{\boldsymbol{r}}_{F_c/B}]\boldsymbol{r}'_{F_c/B} \\ = \boldsymbol{L}_B + m_{\text{sc}}(\ddot{\boldsymbol{r}}_{B/N} \times \boldsymbol{c})\end{aligned} \tag{46}$$

Further simplification of the above equation gives the desired form of the system rotational equations of motion for software implementation:

$$\begin{aligned}m_{\text{sc}}[\tilde{\boldsymbol{c}}]\ddot{\boldsymbol{r}}_{B/N} + [I_{\text{sc},B}]\dot{\boldsymbol{\omega}}_{\mathcal{B}/\mathcal{N}} = \boldsymbol{L}_B - m_{\text{P}}[\tilde{\boldsymbol{r}}_{F_c/B}]\boldsymbol{r}''_{F_c/B} - \left([I'_{\text{sc},B}] + [\tilde{\boldsymbol{\omega}}_{\mathcal{B}/\mathcal{N}}][I_{\text{sc},B}]\right)\boldsymbol{\omega}_{\mathcal{B}/\mathcal{N}} \\ - \left([I'_{\text{P},F_c}] + [\tilde{\boldsymbol{\omega}}_{\mathcal{B}/\mathcal{N}}][I_{\text{P},F_c}]\right)\boldsymbol{\omega}_{\mathcal{F}/\mathcal{B}} - [I_{\text{P},F_c}]\boldsymbol{\omega}'_{\mathcal{F}/\mathcal{B}} - m_{\text{P}}[\tilde{\boldsymbol{\omega}}_{\mathcal{B}/\mathcal{N}}][\tilde{\boldsymbol{r}}_{F_c/B}]\boldsymbol{r}'_{F_c/B}\end{aligned} \tag{47}$$

SOFTWARE IMPLEMENTATION

The open-source Basilisk astrodynamics software package is chosen to simulate the derived multi body dynamics. The modular dynamics architecture of Basilisk utilizes the elegant backsubstitution method developed in prior work by Allard and Schaub which has been shown to solve the critical issues of software maintainability, scalability, and testability while achieving computational efficiency.[12]

The derived multi-body dynamics are implemented in Basilisk as an instance of the `stateEffector` abstract class. To integrate the prescribed dynamics into the modular architecture of Basilisk, the translational and rotational equations of motion of the hub are expressed in the compact manner using Eqs. (19) and (47):

$$\begin{bmatrix} [A] & [B] \\ [C] & [D] \end{bmatrix} \begin{bmatrix} \ddot{\mathbf{r}}_{B/N} \\ \dot{\boldsymbol{\omega}}_{\mathcal{B}/\mathcal{N}} \end{bmatrix} = \begin{bmatrix} \mathbf{v}_{\text{trans}} \\ \mathbf{v}_{\text{rot}} \end{bmatrix} \tag{48}$$

where [A],[B],[C], and [D] are all 3×3 matrices of zeros and

$$\mathbf{v}_{\text{trans}} = \boldsymbol{F}_{ext} - m_{\text{P}} \boldsymbol{r}''_{F_c/B} - 2m_{sc}[\tilde{\boldsymbol{\omega}}_{\mathcal{B}/\mathcal{N}}]\boldsymbol{c}' - m_{sc}[\tilde{\boldsymbol{\omega}}_{\mathcal{B}/\mathcal{N}}]^2\boldsymbol{c} \tag{49}$$

$$\begin{aligned} \mathbf{v}_{\text{rot}} = \boldsymbol{L}_B - m_{\text{P}}[\tilde{\boldsymbol{r}}_{F_c/B}]\boldsymbol{r}''_{F_c/B} - \left([I'_{\text{sc},B}] + [\tilde{\boldsymbol{\omega}}_{\mathcal{B}/\mathcal{N}}][I_{\text{sc},B}]\right)\boldsymbol{\omega}_{\mathcal{B}/\mathcal{N}} \\ - \left([I'_{\text{P},F_c}] + [\tilde{\boldsymbol{\omega}}_{\mathcal{B}/\mathcal{N}}][I_{\text{P},F_c}]\right)\boldsymbol{\omega}_{\mathcal{F}/\mathcal{B}} - [I_{\text{P},F_c}]\boldsymbol{\omega}'_{\mathcal{F}/\mathcal{B}} - m_{\text{P}}[\tilde{\boldsymbol{\omega}}_{\mathcal{B}/\mathcal{N}}][\tilde{\boldsymbol{r}}_{F_c/B}]\boldsymbol{r}'_{F_c/B} \end{aligned} \tag{50}$$

Looking at Eqs. (48-50), it is clear that only the right-hand side of Eq. (48) contains the states of the prescribed body. Therefore, the hub states are directly impacted by the prescribed body's motion. Conversely, the left-hand side of Eq. (48) does not contain any second-order prescribed state variables. This representation confirms that the prescribed states dynamics are not impacted by the hub dynamics.

To simulate the formulated dynamics, a rotational maneuver and a translational maneuver are individually simulated in Basilisk. Two new flight software modules are written to profile the prescribed body's translational and rotational motion. Figure (2) illustrates the Basilisk dynamics architecture and module connections for the translational and rotational simulations.

Rotational Motion Profiler

To validate the derived rotational dynamics, a 1 DOF rotational motion flight software module is written to profile the prescribed body's motion with respect to the mount frame. The inputs to the profiler are the scalar maximum angular acceleration for the attitude maneuver α_{Max}, the prescribed body's initial attitude with respect to the mount frame as the Principal Rotation Vector `prv_F0/M` $(\Phi_0, \hat{\boldsymbol{e}}_0)$, and the prescribed body's reference attitude with respect to the mount frame as the Principal Rotation Vector `prv_F1/M` $(\Phi_1, \hat{\boldsymbol{e}}_1)$. The prescribed body is assumed to be non-rotating at the beginning of the attitude maneuver.

Subtracting the initial principal rotation vector from the reference principal rotation vector gives the required rotation angle and axis for the maneuver:[10]

$$\Phi_{\text{Ref}} = 2\cos^{-1}\left(\cos\frac{\Phi_1}{2}\cos\frac{\Phi_0}{2} + \sin\frac{\Phi_1}{2}\sin\frac{\Phi_0}{2}\hat{\boldsymbol{e}}_1 \cdot \hat{\boldsymbol{e}}_0\right) \tag{51}$$

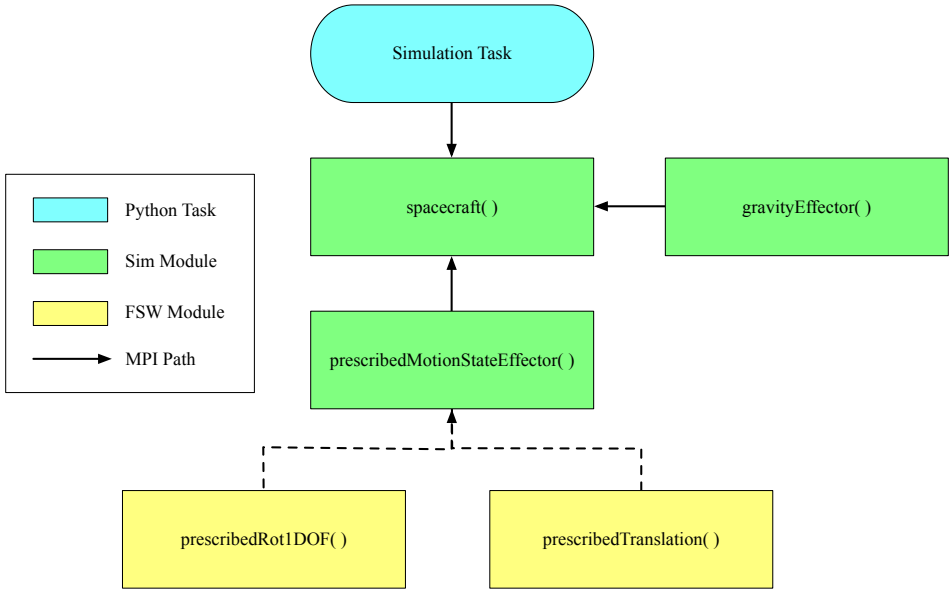

Figure 2. Basilisk dynamics architecture for the simulations.

$$\hat{\boldsymbol{e}} = \frac{\cos\frac{\Phi_0}{2}\sin\frac{\Phi_1}{2}\hat{\boldsymbol{e}}_1 - \cos\frac{\Phi_1}{2}\sin\frac{\Phi_0}{2}\hat{\boldsymbol{e}}_0 + \sin\frac{\Phi_1}{2}\sin\frac{\Phi_0}{2}\hat{\boldsymbol{e}}_1 \times \hat{\boldsymbol{e}}_0}{\sin\frac{\Phi_{\text{Ref}}}{2}} \tag{52}$$

During the first half of the attitude maneuver, the prescribed body is constantly accelerated with the given maximum angular acceleration. The prescribed body's angular velocity increases linearly during the acceleration phase and reaches a maximum magnitude halfway through the attitude maneuver. The switch time t_s is the simulation time halfway through the maneuver:

$$t_s = t_0 + \frac{\Delta t}{2} \tag{53}$$

where the time required for the maneuver Δt is determined using the inputs to the profiler:

$$\Delta t = t_f - t_0 = 2\sqrt{\frac{\Phi_{\text{Ref}}}{\ddot{\Phi}_{\text{Max}}}} \tag{54}$$

The resulting trajectory of the angle Φ swept during the first half of the maneuver is quadratic. The profiled motion is concave upwards if the reference angle Φ_{Ref} is greater than zero. If the converse is true, the profiled motion is instead concave downwards. The described motion during the first half of the attitude maneuver is characterized by the expressions:

$$\omega_{\mathcal{F}/\mathcal{M}}(t) = \alpha_{\text{Max}} \tag{55}$$

$$\dot{\Phi}(t) = \alpha_{\text{Max}}(t - t_0) \tag{56}$$

$$\Phi(t) = c_1(t - t_0)^2 \tag{57}$$

where

$$c_1 = \frac{\Phi_{\text{Ref}}}{2(t_s - t_0)^2} \tag{58}$$

Similarly, the second half of the attitude maneuver decelerates the prescribed body constantly until it reaches a non-rotating state. The prescribed body angular velocity decreases linearly from its maximum magnitude back to zero. The trajectory swept during the second half of the maneuver is quadratic and concave downwards if the reference angle Φ_{Ref} is positive. If Φ_{Ref} is negative, the profiled motion is instead concave upwards. The described motion during the second half of the attitude maneuver is characterized by the expressions:

$$\ddot{\Phi}(t) = -\alpha_{\text{Max}} \tag{59}$$

$$\dot{\Phi}(t) = \alpha_{\text{Max}}(t - t_f) \tag{60}$$

$$\Phi(t) = c_2(t - t_f)^2 + \Phi_{\text{Ref}} \tag{61}$$

where

$$c_2 = \frac{\Phi_{\text{Ref}}}{2(t_s - t_f)^2} \tag{62}$$

Linear Motion Profiler

To validate the derived translational dynamics, a translational motion flight software module is written to profile the prescribed body's position with respect to the hub-fixed mount frame. The inputs to the profiler are the scalar maximum acceleration for the maneuver a_{Max}, the mount frame axis for the translational motion, and the prescribed body's initial position vector with respect to the mount frame $\boldsymbol{r}_{F/M_0}$, and the reference position vector or the prescribed body with respect to the mount frame $\boldsymbol{r}_{F/M_{\text{Ref}}}$. The magnitudes of the initial and final position vectors are denoted r_0 and r_{Ref}, respectively. The prescribed body is assumed to be at rest at the beginning of the attitude maneuver.

Subtracting the initial position from the reference position vector gives the required relative position vector in the direction of translation:

$$\Delta\boldsymbol{r} = \boldsymbol{r}_{F/M_{\text{Ref}}} - \boldsymbol{r}_{F/M_0} \tag{63}$$

The magnitude of the determined relative position vector gives the required translational distance Δr. During the first half of the maneuver, the prescribed body is constantly accelerated with the given maximum acceleration. The prescribed body's velocity increases linearly during the acceleration phase and reaches a maximum magnitude halfway through the maneuver. Eq. (53) gives the switch time t_s for the translational maneuver.

The time required for the maneuver Δt is determined using the inputs to the profiler:

$$\Delta t = \sqrt{\frac{4r_{\text{Ref}} - 8r_0}{\ddot{a}_{\text{Max}}}} \tag{64}$$

The resulting trajectory of the position vector $r = ||\boldsymbol{r}_{F/M}||_2$ magnitude during the first half of the maneuver is quadratic. The profiled motion is concave upwards if the reference position magnitude r_{Ref} is greater than the initial position magnitude r_0. If the converse is true, the profiled motion is instead concave downwards. The described motion during the first half of the maneuver is characterized by the expressions:

$$r''_{F/M}(t) = a_{\text{Max}} \tag{65}$$

$$r'_{F/M}(t) = a_{\text{Max}}(t - t_0) \tag{66}$$

$$r_{F/M}(t) = c_3(t - t_0)^2 + r_0 \tag{67}$$

where

$$c_3 = \frac{r_{\text{Ref}} - r_0}{2(t_s - t_0)^2} \tag{68}$$

Similarly, the second half of the maneuver decelerates the prescribed body constantly until it reaches the desired position with zero velocity. The prescribed body velocity decreases linearly from its maximum magnitude back to zero. The trajectory during the second half of the maneuver is quadratic and concave downwards if the reference position magnitude is greater than the initial position magnitude. If the converse is true, the profiled motion is instead concave upwards. The described motion during the second half of the maneuver is characterized by the expressions:

$$r''_{F/M}(t) = -a_{\text{Max}} \tag{69}$$

$$r'_{F/M}(t) = a_{\text{Max}}(t - t_f) \tag{70}$$

$$r_{F/M}(t) = c_4(t - t_f)^2 + r_{\text{Ref}} \tag{71}$$

where

$$c_4 = \frac{r_{\text{Ref}} - r_0}{2(t_s - t_f)^2} \tag{72}$$

RESULTS

Simulation Setup

The simulation sets up an initially non-rotating cylindrical spacecraft hub with a mass of 750 kilograms in a circular orbit about the Earth. The Earth-Centered Inertial (ECI) frame is the chosen inertial frame of reference for the simulation. The hub body frame is initially aligned with the inertial frame. The hub states for both maneuvers are listed in Table (1). The inertia of the hub about its center of mass is taken to be:

$$^{B}[I_{\text{hub},B_c}] = \begin{bmatrix} 900 & 0.0 & 0.0 \\ 0.0 & 800 & 0.0 \\ 0.0 & 0.0 & 600 \end{bmatrix} \text{ kg} \cdot \text{m}^2 \tag{73}$$

The prescribed body is given a cubic geometry with a mass of 100 kilograms and moment of inertia about its center of mass:

$$^{F}[I_{\text{P},F_c}] = \begin{bmatrix} 50 & 0.0 & 0.0 \\ 0.0 & 50 & 0.0 \\ 0.0 & 0.0 & 50 \end{bmatrix} \text{ kg} \cdot \text{m}^2 \tag{74}$$

The prescribed body's initial states and mass properties are given in Table (2). The reference states for the rotational and translational maneuvers are listed in Table (3) and Table (4), respectively.

Table 1. Initial hub states.

Parameter	Value	Unit
m_{hub}	750	kg
${}^{B}[I_{\text{hub},B_c}]$	$\begin{bmatrix} 900 & 0.0 & 0.0 \\ 0.0 & 800 & 0.0 \\ 0.0 & 0.0 & 600 \end{bmatrix}$	kg $\cdot$ m^2
$\boldsymbol{r}_{B_c/B}(t_0)$	[0.0, 0.0, 0.0]	m
$\boldsymbol{r}_{C/N}(t_0)$	[-4020338.690, 7490566.741, 5248299.211]	m
$\boldsymbol{v}_{C/N}(t_0)$	[-5199.777, -3436.681, 1041.576]	m
$\omega_{\mathcal{B}/\mathcal{N}}(t_0)$	[0.0, 0.0, 0.0]	deg/s
$\boldsymbol{\sigma}_{\mathcal{B}/\mathcal{N}}(t_0)$	[0.0, 0.0, 0.0]	N/A

Table 2. Initial prescribed body states.

Parameter	Value	Unit
m_{P}	100	kg
${}^{F}[I_{\text{P},F_c}]$	$\begin{bmatrix} 50 & 0.0 & 0.0 \\ 0.0 & 50 & 0.0 \\ 0.0 & 0.0 & 50 \end{bmatrix}$	kg $\cdot$ m^2
$\boldsymbol{r}_{F_c/F}(t_0)$	[0.0, 0.0, 0.0]	m
$\boldsymbol{r}_{M/B}(t_0)$	[0.0, 0.0, 0.0]	m
$\boldsymbol{r}_{F/M}(t_0)$	[0.0, 0.0, 0.0]	m
$\boldsymbol{r}'_{F/M}(t_0)$	[0.0, 0.0, 0.0]	m/s
$\boldsymbol{r}''_{F/M}(t_0)$	[0.0, 0.0, 0.0]	m/s^2
$\omega_{\mathcal{M}/\mathcal{B}}(t_0)$	[0.0, 0.0, 0.0]	deg/s
$\boldsymbol{\omega}_{\mathcal{F}/\mathcal{M}}(t_0)$	[0.0, 0.0, 0.0]	deg/s
$\boldsymbol{\omega}'_{\mathcal{F}/\mathcal{M}}(t_0)$	[0.0, 0.0, 0.0]	deg/s^2
$\boldsymbol{\sigma}_{\mathcal{F}/\mathcal{M}}(t_0)$	[0.0, 0.0, 0.0]	N/A
Φ_0	0.0	deg
r_0	0.0	m

Table 3. Reference prescribed body states for the rotational maneuver.

Parameter	Value	Unit
Φ_{Ref}	30.0	deg
$\boldsymbol{\sigma}_{\mathcal{F}/\mathcal{M}}$(Ref)	[0.1316525, 0.0, 0.0]	N/A
$\omega'_{\mathcal{F}/\mathcal{M}\text{ Max}}$	1.0	deg/s^2
RotsAxis	[1.0, 0.0, 0.0]	N/A

Table 4. Reference prescribed body states for the translational maneuver.

Parameter	Value	Unit
r_{Ref}	0.5	m
$\boldsymbol{r}_{F/M}$(Ref)	[0.25, 0.0, 0.4330127]	m
$r''_{F/M\text{ Max}}$	$2.5e^{-4}$	m/s^2
TransAxis	[0.5, 0.0, $\sqrt{3}$ / 2]	N/A

Rotational Motion Simulation Results

The rotational simulation results are given in Figs. (3) and (4). Figure (3) presents the profiled prescribed motion in subplots (a-c) and the resulting spacecraft hub motion in subplots(b-f). The prescribed body converges to the reference angle in 11.2 seconds as a result of the chosen angular acceleration profile. Accordingly, the profiled angular velocity is linear, reaching a maximum magnitude of 5.4544 deg/s halfway through the maneuver. The hub is expected to rotate oppositely to the profiled rotation to maintain conservation of the system angular momentum. Subplots (b) and (d) confirm this expected behavior. The orbital position of the hub with respect to the inertial frame seen in subplot (d) does not visibly change due to the small period of time required for the maneuver.

Figure (4) displays the changes in the four quantities of orbital angular momentum, orbital energy, rotational angular momentum, and rotational energy for this simulation. The orbital quantities describe the movement of the spacecraft center of mass in orbit. The rotational quantities describe the rotation of the spacecraft about its center of mass. For a purely rotational maneuver, the orbital angular momentum, orbital energy, and spacecraft rotational angular momentum will be conserved. Subplots (a) and (c) confirm the orbital and rotational angular momentum quantities are conserved. However, in the software implementation the prescribed parameters are held fixed at the dynamics integration level, resulting in the orbital energy being nearly conserved as seen in subplot (b). The spacecraft rotational energy is not expected to be conserved because the positive and negative acceleration segments of the maneuver add and remove energy from the system, respectively. Subplot (d) validates the described expected results for the spacecraft rotational energy. The spacecraft returns to a state of zero rotational energy at the end of the maneuver.

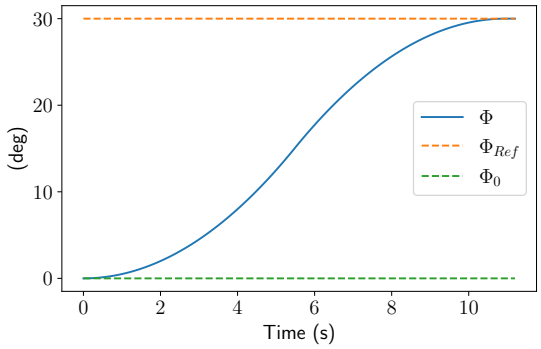

(a) Prescribed Body Angle $\boldsymbol{\Phi}_{F/M}$.

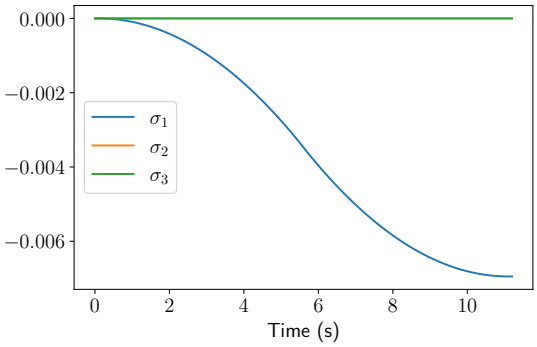

(b) Hub Attitude $\boldsymbol{\sigma}_{B/N}$.

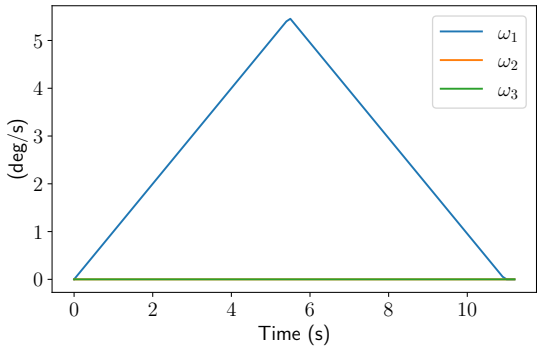

(c) Prescribed Body Angular Velocity ${}^{F}\boldsymbol{\omega}_{\mathcal{F}/\mathcal{M}}$.

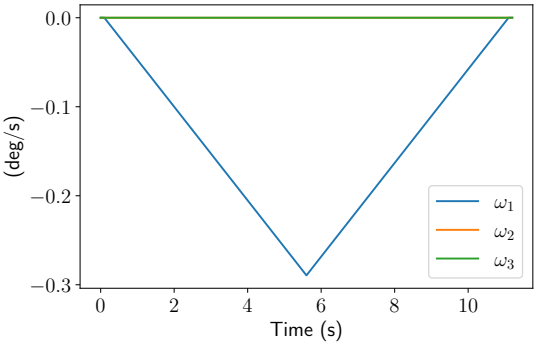

(d) Hub Angular Velocity ${}^{B}\boldsymbol{\omega}_{\mathcal{B}/\mathcal{N}}$.

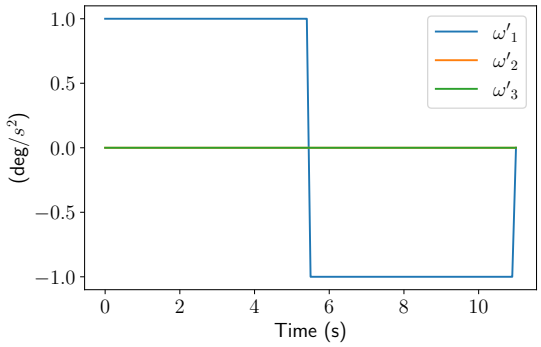

(e) Prescribed Body Angular Acceleration ${}^{F}\boldsymbol{\omega}'_{\mathcal{F}/\mathcal{M}}$.

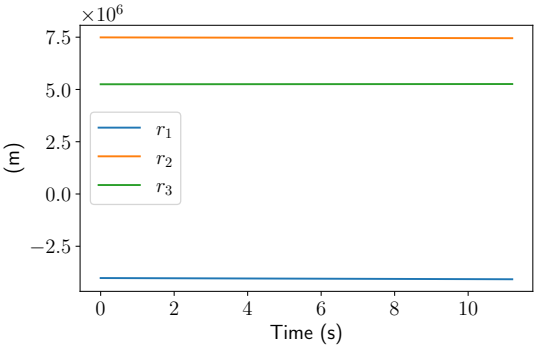

(f) Hub Position ${}^{N}\boldsymbol{r}_{B/N}$.

Figure 3. Kinematic states of the prescribed body and spacecraft hub for the rotational maneuver.

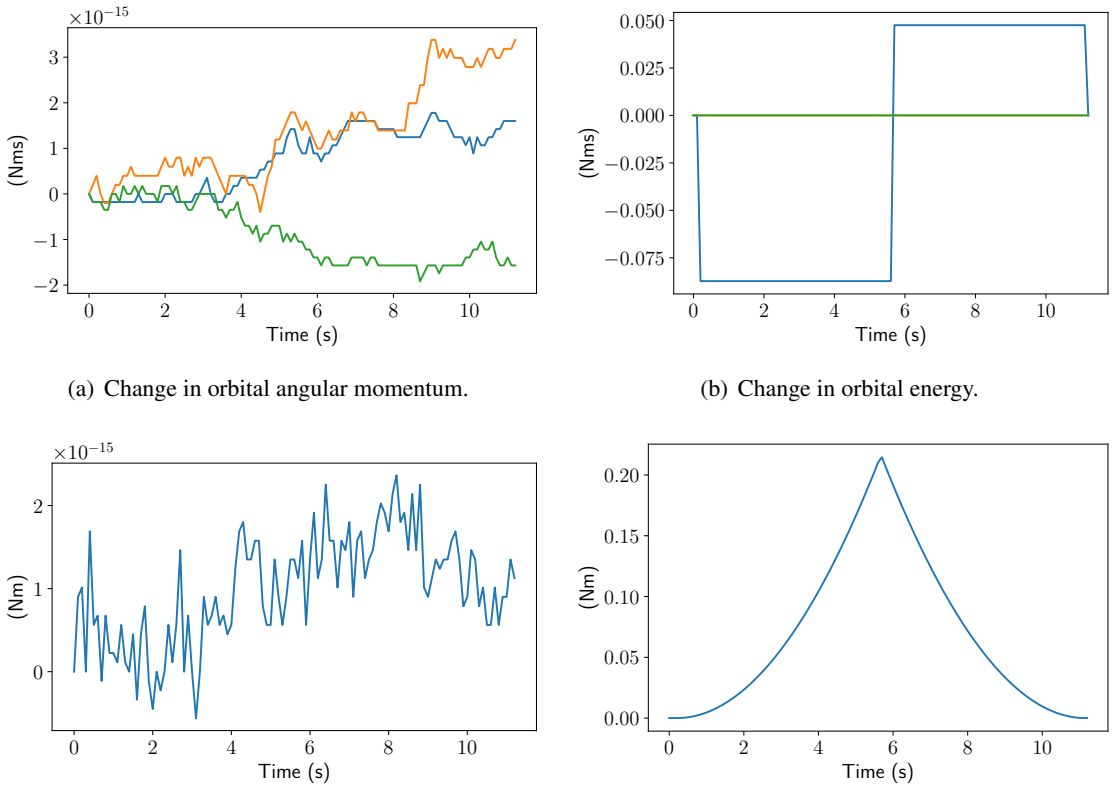

(a) Change in orbital angular momentum.

(b) Change in orbital energy.

(c) Change in rotational angular momentum.

(d) Change in rotational energy.

Figure 4. Conservation of angular momentum and energy for the rotational maneuver.

Linear Motion Simulation Results

The simulation results for the translational maneuver can be seen in Figs. (5) and (6). The profiled prescribed motion is presented in subplots (a-c) of Fig. (5) and the resulting spacecraft hub motion in provided in subplots(b-f). The prescribed body is seen to converge to the reference position in 89.5 seconds as a result of the chosen acceleration profile. Accordingly, the profiled velocity is linear, reaching a maximum magnitude of 11.17 mm/s halfway through the maneuver. Because the maneuver is purely translational, the hub is expected to remain in a non-rotating state. Subplots (d) and (f) confirm this expected behavior. The hub attitude and angular velocity with respect to the inertial frame are both seen to remain unchanged. The small changes in the hub position with respect to the inertial frame seen in subplot (b) are an expected result of the orbital motion of the spacecraft about the Earth.

Figure (6) displays the changes in the four quantities of orbital angular momentum, orbital energy, rotational angular momentum, and rotational energy for this simulation. For a purely translational maneuver, the orbital angular momentum, orbital energy, and spacecraft rotational angular momentum will be conserved. However, in the software implementation the prescribed parameters are held fixed at the dynamics integration level, resulting in the expected quantities being nearly conserved as seen in subplots (a-c). The spacecraft rotational energy is not expected to be conserved for the translational case because the positive and negative acceleration segments of the maneuver add and remove energy from the system, respectively. Subplot (d) validates the described expected results

for the spacecraft rotational energy. The spacecraft returns to a state of zero rotational energy at the end of the maneuver.

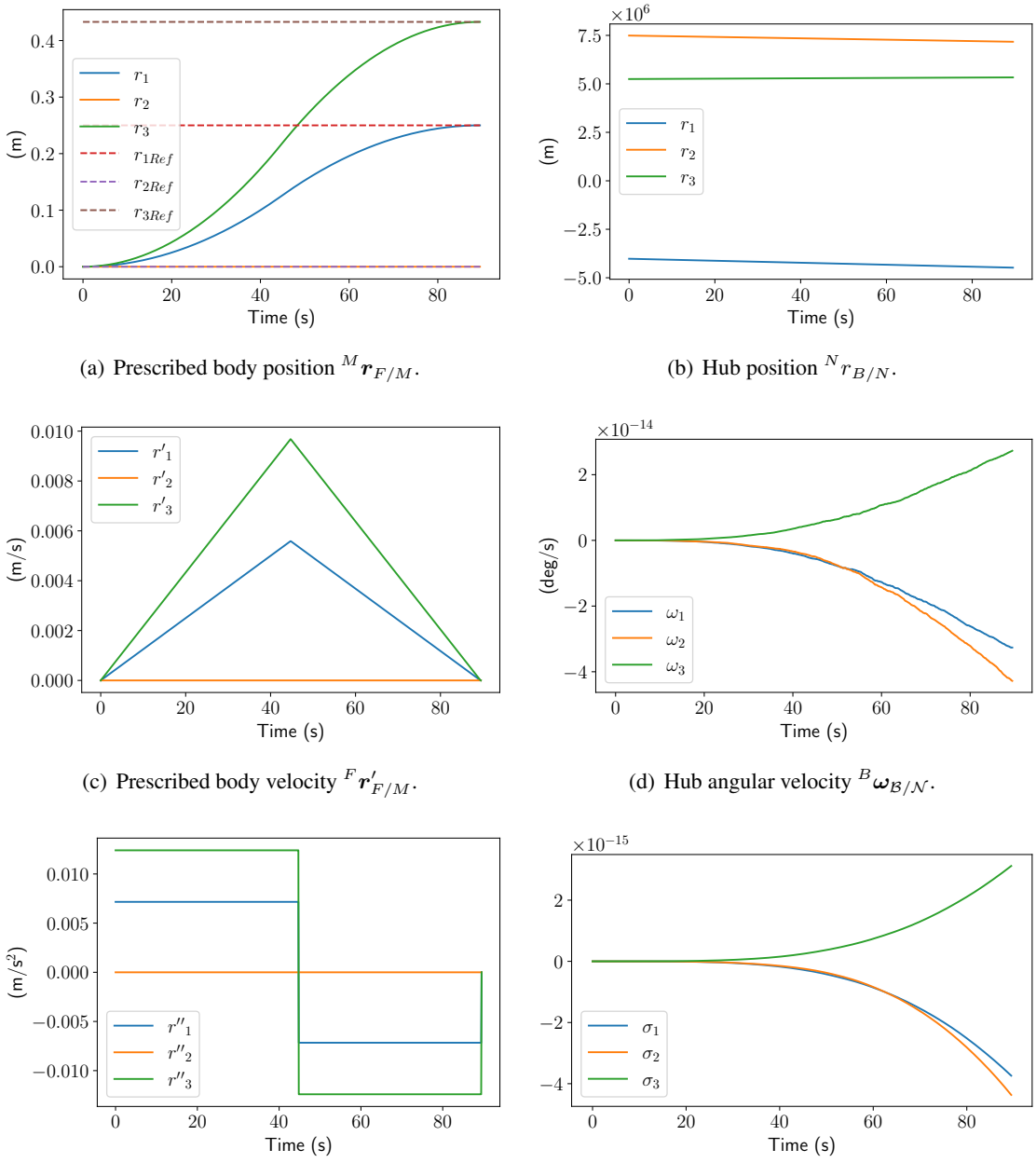

(a) Prescribed body position ${}^{M}\boldsymbol{r}_{F/M}$.

(b) Hub position ${}^{N}r_{B/N}$.

(c) Prescribed body velocity ${}^{F}\boldsymbol{r}'_{F/M}$.

(d) Hub angular velocity ${}^{B}\boldsymbol{\omega}_{\mathcal{B}/\mathcal{N}}$.

(e) Prescribed body acceleration ${}^{F}\boldsymbol{r}''_{F/M}$.

(f) Hub attitude $\boldsymbol{\sigma}_{B/N}$.

Figure 5. Kinematic states of the prescribed body and spacecraft hub for the translational maneuver.

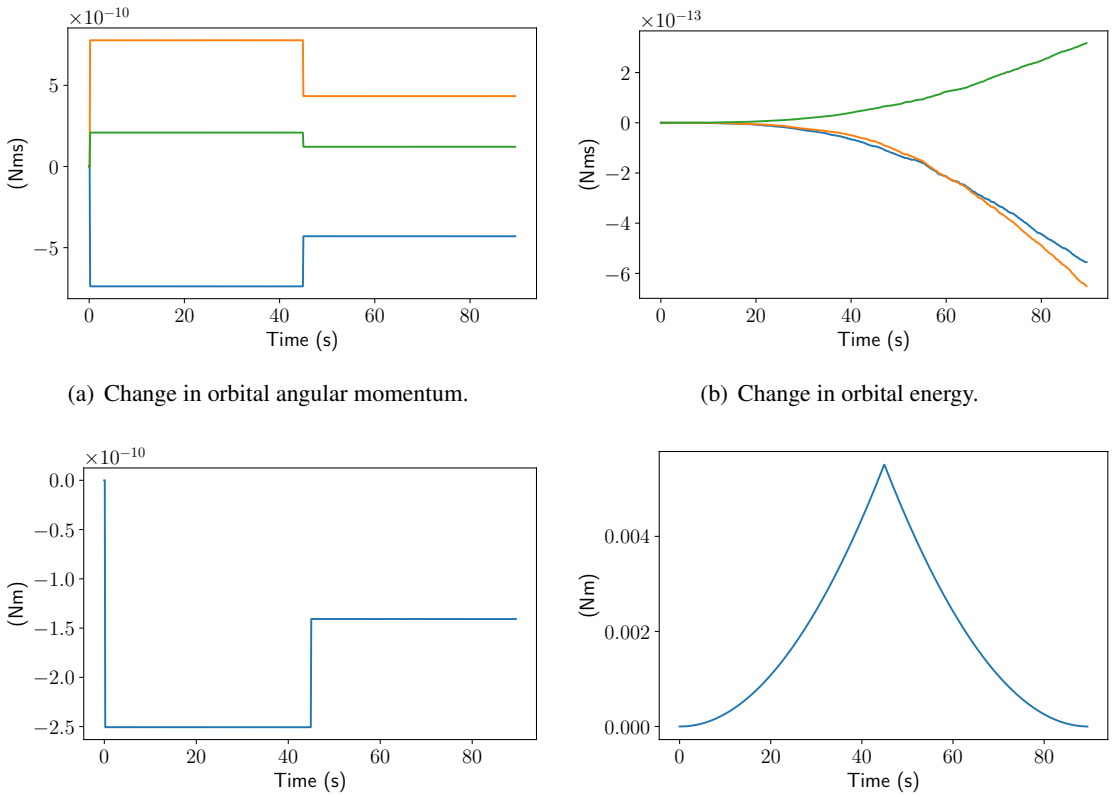

(a) Change in orbital angular momentum.

(b) Change in orbital energy.

(c) Change in rotational angular momentum.

(d) Change in rotational energy.

Figure 6. Conservation of angular momentum and energy for the translational maneuver.

CONCLUSION

A multi-body dynamics model for general six-degree of freedom motion of a rigid prescribed body connected to a spacecraft hub was developed using an angular momentum-based equation of motion development. The derived dynamics were implemented in the Basilisk software for a prescribed body following both translational and rotational prescribed motion with respect to the spacecraft hub. The conservation quantities of orbital angular momentum, orbital energy, rotational angular momentum, and rotational energy are checked for conservation. The obtained results give confidence that the derivation presented is valid.

REFERENCES

[1] C. Allard, H. Schaub, and S. Piggott, "General Hinged Rigid-Body Dynamics Approximating First-Order Spacecraft Solar Panel Flexing," *Journal of Spacecraft and Rockets*, Vol. 55, No. 5, 2018, pp. 1290–1298.

[2] Y. Cao, D. Cao, J. Wei, and W. Huang, "Attitude Dynamics of Satellites with Flexible Appendages—A Brief Review," *Journal of Aerospace Science and Technology*, Vol. 84, 2019, pp. 131–142.

[3] A. Jain and G. Rodriguez, "Recursive Dynamics Algorithm for Multibody Systems with Prescribed Motion," *Journal of Guidance, Control, and Dynamics*, Vol. 16, No. 5, 1993, pp. 830–837.

[4] A. K. Banerjee, "Contributions of Multibody Dynamics to Space Flight: A Brief Review," *Journal of Guidance, Control, and Dynamics*, Vol. 26, No. 3, 2003, pp. 385–394.

[5] V. J. Modi, "Attitude Dynamics of Satellites with Flexible Appendages—A Brief Review," *Journal of Spacecraft and Rockets*, Vol. 11, No. 11, 1974, pp. 743–751.

[6] A. Jain, "Unified Formulation of Dynamics for Serial Rigid Multibody System," *Journal of Guidance, Control, and Dynamics*, Vol. 14, No. 3, 1991, pp. 531–542.

[7] H. A. Ardakani and T. J. Bridges, "Dynamic Coupling Between Shallow-water Sloshing and a Vehicle Undergoing Planar Rigid-body Motion," 2010, pp. –.

[8] J. Gerrits and A. Veldman, "Dynamics of liquid-filled spacecraft," *Journal of Engineering Mathematics.*, Vol. 45, No. 1, 2003, pp. 21–38.

[9] A. Veldman, J. Gerrits, R. Luppes, J. Helder, and J. Vreeburg, "The numerical simulation of liquid sloshing on board spacecraft,," *Journal of Computational Physics*, Vol. 224, No. 1, 2007, pp. 82–99.

[10] H. Schaub and J. L. Junkins, *Analytical Mechanics of Space Systems*. Reston, Virginia: American Institute of Aeronautics and Astronautics, Inc., 4 ed., 2018.

[11] C. Allard, J. Maxwell, and H. Schaub, "A Transport Theorem for the Inertia Tensor for Simplified Spacecraft Dynamics Development," International Astronautical Conference, Paris, France, Sept. 18-22, 2022.

[12] C. Allard, M. D. Ramos, H. Schaub, P. Kenneally, and S. Piggott, "Modular Software Architecture for Fully Coupled Spacecraft Simulations," *Journal of Aerospace Information Systems*, Vol. 15, No. 12, 2018, pp. 670–683.